

# A pulsed Sagnac source of narrowband polarization-entangled photons

Onur Kuzucu and Franco N. C. Wong

*Research Laboratory of Electronics, Massachusetts Institute of Technology, Cambridge, Massachusetts 02139, USA*

(Dated: October 29, 2018)

We demonstrate pulsed operation of a bidirectionally pumped polarization Sagnac interferometric down-conversion source and its generation of narrowband, high-visibility polarization-entangled photons. Driven by a narrowband, mode-locked pump at 390.35 nm, the phase-stable Sagnac source with a type-II phase-matched periodically poled KTiOPO<sub>4</sub> crystal is capable of producing 0.01 entangled pair per pulse in a 0.15-nm bandwidth centered at 780.7 nm with 1 mW of average pump power at a repetition rate of 31.1 MHz. We have achieved a mean photon-pair generation rate of as high as 0.7 pair per pulse, at which multi-pair events dominate and significantly reduce the two-photon quantum-interference visibility. For low generation probability  $\alpha$ , the reduced visibility  $V = 1 - \alpha$  is independent of the throughput efficiency and of the polarization analysis basis, which can be utilized to yield an accurate estimate of the generation rate  $\alpha$ . At low  $\alpha$  we have characterized the source entanglement quality in three different ways: average quantum-interference visibility of 99%, the Clauser-Horne-Shimony-Holt  $S$  parameter of  $2.739 \pm 0.119$ , and quantum state tomography with 98.85% singlet-state fidelity. The narrowband pulsed Sagnac source of entangled photons is suitable for use in quantum information processing applications such as free-space quantum key distribution.

PACS numbers: 03.67.Mn, 42.65.Lm, 42.50.Dv, 03.65.Wj

## I. INTRODUCTION

Photonic entanglement is an essential resource for many quantum information processing applications, such as linear-optics quantum computing (LOQC) [1], quantum teleportation [2], and quantum key distribution (QKD) [3]. The most widely used method for generating polarization-entangled photon pairs is spontaneous parametric down-conversion (SPDC), which can be realized in a number of configurations and by using different crystals [4, 5, 6, 7, 8, 9, 10, 11]. A well optimized SPDC source with high flux and high entanglement quality can be utilized to develop advanced enabling quantum technology such as a random number generator [12]. Certain applications such as quantum communications and LOQC are often designed to operate with a system clock to allow for synchronization and, for that purpose, a pulsed source of entangled photons is needed. In other applications such as free-space entanglement-based QKD in the daylight, pulsed operation may be preferred to simplify signaling of the arrival times of the entangled photons and to provide temporal discrimination against undesirable background light. Many SPDC sources, however, are continuous-wave (cw) pumped which cannot yield any timing information about when an entangled photon pair is generated. It is therefore of interest to develop an efficient pulsed source of entangled photons that can offer unique operational and application-specific advantages over a cw SPDC source.

We have previously developed a cw SPDC source of polarization-entangled photons using a polarization Sagnac interferometer (PSI) configuration that is highly efficient and yields a high visibility in two-photon quantum interference [7, 8]. The Sagnac source configuration is a phase-stable, single-crystal implementation

of interferometrically combined outputs of two identical, coherently-driven down-converters [13, 14]. The PSI configuration eliminates the need for spatial (aperture), spectral (interference filter), and temporal (timing compensator) filtering because the two down-converter outputs are completely indistinguishable [5]. All the output photons are strongly polarization-entangled without the need for filtering, thus leading to a much higher generation efficiency than that of other approaches.

In principle, the Sagnac configuration can be used for both cw and pulsed operation. Shi and Tomita have previously utilized a non-polarizing Sagnac interferometer to realize a highly stable pulsed down-conversion entanglement source [15]. The use of a non-polarizing beam splitter incurs a 50% reduction in the entanglement generation rate because when both photons exit the same port of the beam splitter (half of the time) it does not produce polarization entanglement. In this work, we employ a polarizing beam splitter (PBS) to eliminate this 50% loss, and we demonstrate the first pulsed operation of a Sagnac down-conversion source pumped by a narrowband, mode-locked ultraviolet (UV) source. Unlike most pulsed SPDC sources that are pumped by femtosecond lasers [10, 11], the pulsed Sagnac source is pumped with  $\sim 50$ -ps pulses with a narrow spectral bandwidth. While the cw and pulsed Sagnac sources share a common design, there can be major differences between the two types of sources. In cw down-conversion the output flux is often limited by available cw pump power, especially in the UV region. Therefore cw sources are often characterized by a normalized generation efficiency in terms of the number of entangled pairs generated per second per nanometer of detection bandwidth for 1 mW of pump power. In general, the situation is different for pulsed pumping because high peak power is easily obtainable at many wavelengths, either directly from a laser or

by efficient harmonic generation of a high power pulsed laser [16]. The high peak pump power for pulsed down-conversion benefits applications that can take advantage of a substantial pair generation probability per pulse such as those requiring multiphoton coincidences for the generation of novel multipartite states in LOQC [17, 18]. On the other hand, with high generation probabilities one must be careful with the impact of multiple-pair events on the system performance of some quantum information processing applications. For instance, in free-space entanglement-based QKD the entanglement source may be strongly driven to achieve a desirable key generation rate but it should not exceed a level that may compromise the security of the generated secret keys [19].

We have developed a pulsed Sagnac source based on type-II phase-matched periodically poled  $\text{KTiOPO}_4$  (PPKTP) and pumped with a custom-built high-power mode-locked UV source at 390.35 nm [16]. The Sagnac source is capable of producing polarization-entangled photon pairs at 780.7 nm with a mean pair generation of as much as one per pulse, even in a small bandwidth of 0.15 nm. The narrowband pulsed Sagnac source is particularly suitable for free-space entanglement-based QKD. Pulsed operation affords synchronized detection of the entangled photons and provides temporal discrimination against temporally random background photons or detector dark counts. The narrowband outputs can be used with narrowband spectral filtering that is essential for blocking out ambient light during daylight operation.

In the next section, we describe our experimental setup in the construction of the pulsed Sagnac source. In section III, we characterize the entanglement quality of the PSI output with three different types of measurements: two-photon quantum interference, violation of Clauser-Horne-Shimony-Holt (CHSH) form of Bell's inequality [20], and quantum state tomography. In section IV, we focus on the strongly pumped Sagnac source with its high-flux outputs and the accompanying visibility degradation due to occurrence of multiple-pair events, before concluding in section V.

## II. EXPERIMENTAL SETUP

We develop the narrowband pulsed Sagnac source for potential use in free-space entanglement-based QKD that must satisfy a number of operational constraints. For line-of-sight free-space QKD it has been suggested that the optimal operating wavelength is around 780 nm that takes into account atmospheric transmission and the characteristics of commercially available Si avalanche photodiodes (APDs) as single-photon counters [21]. Commercially available Si APDs typically have a detection quantum efficiency of  $\sim 50\%$  and a rise time of  $\sim 300$  ps. The pump for the Sagnac source should have a pulse width that is small compared with the detector rise time so that the pump does not add to the timing uncertainty. At the same time, we prefer to operate the

down-converter in a quasi-cw manner with a pump bandwidth that is small compared with the down-conversion phase-matching bandwidth or the spectral filter bandwidth. Otherwise, some of the photon pairs generated by the broadband pump would be outside of the measurement bandwidth and the system throughput efficiency is reduced. We choose the pump requirements to have a pulse width of 100 ps or less and a bandwidth of less than 0.1 nm. A narrowband down-conversion output allows the use of narrowband spectral filters inserted before the Si APD detectors to screen out background light from the sky during daylight QKD operation. The pulse width and bandwidth requirements can accommodate a range of pump operating conditions and we note that transform limited pulses are not required.

Figure 1 shows the experimental setup for the pulsed Sagnac source together with the measurement apparatus. We will briefly describe the PSI configuration and more details can be found in previous cw implementations [7, 8, 9]. The PSI, as shown in the dashed box of Fig. 1, is composed of two flat mirrors and a PBS that serves as the input and output optical element. Within the interferometer is a nonlinear crystal for generating entangled photons by SPDC. Bidirectional pumping of the crystal in counter-propagating directions creates coherent superposition of the counter-propagating down-conversion outputs at the PBS, whose output photons are entangled in polarization. Interferometric combination of two outputs is usually sensitive to path-length perturbations, but the PSI configuration eliminates the need for path-length stabilization through its common path arrangement [7]. Moreover, the phase of the output state can be chosen by simply adjusting the relative phase between the horizontally ( $H$ ) and vertically ( $V$ ) polarized components of the pump.

For our pulsed Sagnac source, we used a 10-mm long flux-grown PPKTP crystal from Raicol with a grating period of  $7.85 \mu\text{m}$  for type-II phase matching and degenerate wavelength output at 780.7 nm. The crystal was temperature stabilized at a phase-matching temperature of  $28.6^\circ\text{C}$  using a thermoelectric heater with a temperature stability of better than  $0.1^\circ\text{C}$ . Using cw second-harmonic generation, we measured an effective nonlinear coefficient,  $d_{\text{eff}} = (2/\pi)d_{24}$  of  $\sim 2.4 \text{ pm/V}$ . To ensure that the counter-propagating pump components reach the crystal at the same time, thus eliminating any temporal distinguishability between the two outputs, we positioned the crystal at the center of the interferometer within  $\sim 1$  mm, which is much less than that spanned by the 50-ps pump pulse.

The pulsed UV pump centered at 390.35 nm was a compact, home-built narrowband picosecond UV source based on frequency quadrupling of an amplified mode-locked fiber laser [16]. It had a bandwidth of less than 0.1 nm, full-width at half maximum (FWHM). The passively mode-locked erbium-doped fiber laser with a narrowband intracavity filter was operated at 1561.4 nm at a repetition rate of 31.1 MHz. The fiber laser output was

amplified with a 5-W polarization-maintaining erbium-doped fiber amplifier and followed by two stages of single-pass second-harmonic generation to yield the pulsed UV output with a maximum average power of 400 mW and a pulse width of  $\sim 50$  ps. Because of the frequency quadrupling configuration, there was a significant amount of residual 780.7 nm light in the UV source output. As a UV pump for the Sagnac source, it was necessary to filter this undesirable near-infrared (near-IR) light before reaching the PSI. We used a pair of dichroic mirrors (DMs) that were highly transmissive at 780.7 nm and highly reflective at 390.35 nm, and constructed a 7-bounce passage for the pump beam to filter the residual 780.7 nm light. We estimate that a suppression of 140 dB was achieved using this multiple-bounce dichroic mirror pair arrangement with negligible loss of UV power.

The linearly polarized, collimated UV beam after the DM filter was passed through a half-wave plate (HWP) and a quarter-wave plate (QWP) to adjust the relative phase and amplitude between the  $H$ - and  $V$ -polarized components. We focused the pump into the PSI using a plano-convex lens with a 15-cm focal length and with broadband anti-reflection (AR) coating that covered both UV and near-IR wavelengths. The PPKTP crystal was centered at the pump focal spot that was measured to have a beam diameter of  $\sim 90$   $\mu\text{m}$ . The Sagnac configuration calls for an input/output PBS that works at both the pump and down-conversion wavelengths. Instead, we used a commercially available standard PBS cube designed and AR-coated for 780 nm but not for 390 nm. The PBS provided acceptable extinction ratio ( $\sim 20:1$ ) to separate the  $H$  and  $V$  components of the UV pump, with absorption and reflection losses of 35% at 390 nm. The PBS served to produce counter-propagating pumps for bidirectional pumping of the down-conversion crystal. An AR-coated dual-wavelength half-wave plate (DW-HWP) designed for 390.35 nm and 780.7 nm rotated the  $V$ -polarized pump to  $H$  polarization that was required (along the crystal's  $y$ -axis) for type-II phase matching. We note that the low extinction ratio PBS introduced a small amount of  $V$ -polarized pump at the crystal but it was not phase matched to generate any down-converted photon pairs. Before the signal and idler outputs from the two bidirectionally pumped down-converters were combined at the PBS, the clockwise circulating output was rotated by  $90^\circ$  with the DW-HWP such that the signal and idler beams after the PBS were spatially separated, as indicated in Fig. 1.

Each of the signal and idler outputs was collimated with a 15-cm focal length plano-convex lens and passed through a matching circular aperture for spatial-mode filtering. We sent the output beams to polarization analyzers each comprising a HWP and a high-extinction polarizer to measure the polarization states. A QWP could also be added for quantum state tomography measurements. We filtered both beams spectrally using interference-filters (IFs) with a FWHM bandwidth of  $\sim 0.15$  nm centered at 780.7 nm and with peak transmis-

sion of 60%. The outputs were subsequently focused onto two PerkinElmer Si APDs with  $\sim 50\%$  detection efficiency. We recorded individual APD counts as well as coincidence counts and a 1.8-ns coincidence window was used [22].

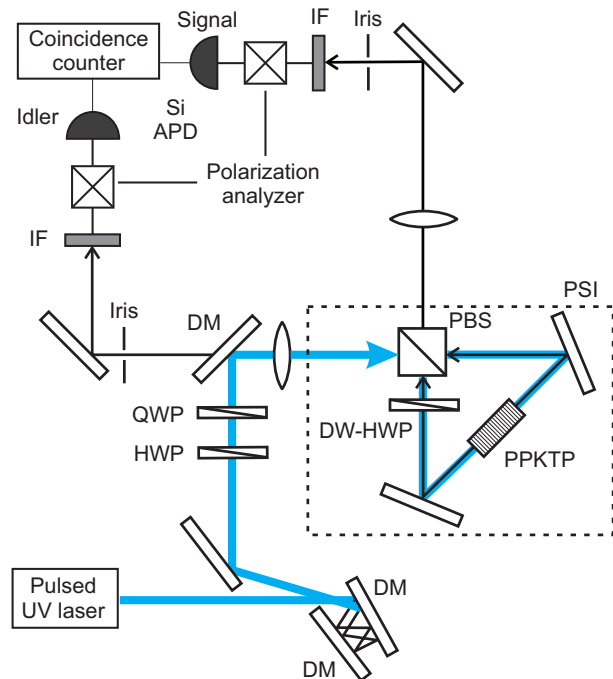


FIG. 1: (Color online) Experimental setup showing the bidirectionally pumped polarization Sagnac interferometer (PSI) in the dashed box. The generated polarization-entangled signal and idler outputs are analyzed in coincidence measurements under different operating conditions. IF, interference filter; PBS, polarizing beam splitter; DM, dichroic mirror; HWP, half-wave plate; QWP, quarter-wave plate; DW-HWP, dual-wavelength half-wave plate.

We aligned the Sagnac interferometer such that the two down-converter outputs for the signal (and for the idler) were spatially and temporally overlapped at the PBS output to erase any "which-path" information. This required symmetric positioning of the PPKTP crystal inside the Sagnac interferometer. At this point, the pair generation rates from both paths were balanced and the necessary input pump polarization adjustments were made to generate a singlet-state output

$$|\psi^-\rangle = (|H_S V_I\rangle - |V_S H_I\rangle)/\sqrt{2}, \quad (1)$$

where the subscript  $S$  ( $I$ ) refers to the signal (idler) photon. In the next two sections, we show the results of our source characterization in the low and high flux regimes.

### III. LOW-FLUX CHARACTERISTICS

Unlike most cw SPDC sources, the combination of a high-power pulsed UV pump and the efficient PSI source

can lead to a substantial pair generation probability per pulse. In order to assess the entanglement quality of the pulsed Sagnac source with minimal degradation due to multiple-pair events, we measured the characteristics of the PSI output at low pumping powers. In particular, we made measurements of the two-photon quantum interference, the CHSH form of Bell's inequality, and quantum state tomography of the PSI output state. We show that the three types of characterization methods are consistent with each other.

### A. Quantum interference visibility

The signal-idler quantum interference measurement in two incompatible polarization bases,  $H-V$  and  $\pm 45^\circ$  antidiagonal-diagonal ( $A-D$ ), is a common and relatively simple method to assess the entanglement quality of the source. For each of the polarization measurement bases, the signal polarization analyzer angle is set at one of the basis polarization axes and the coincidence counts are monitored as a function of the idler analyzer angle. The quantum-interference visibility is given by

$$V = \frac{C_{\max} - C_{\min}}{C_{\max} + C_{\min}}, \quad (2)$$

where  $C_{\max}$  and  $C_{\min}$  are the maximum and minimum coincidence counts, respectively, and an ideal entanglement source yields  $V = 1$ .

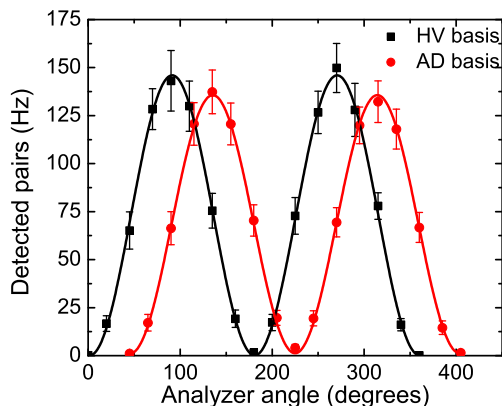


FIG. 2: (Color online) Quantum interference measurements for input pump of 0.1 mW and sinusoidal fits in the  $H-V$  (squares) and  $A-D$  (circles) bases.  $H-V$  ( $A-D$ ) visibility is 99.79% (98.11%).

We observed the quantum interference fringes at different pump power levels and different aperture sizes. Figure 2 shows the coincidence counts in the  $H-V$  and  $A-D$  bases and the corresponding sinusoidal fits to data at a pump power of 0.1 mW, as measured at the entrance to the PSI. Each data point represents an average of 30 1-s measurements, and we apply no background-count subtraction to the coincidence count data in Fig. 2. Using the measured maximum and minimum coincidence

counts we obtain from Eq. (2) an interference visibility of  $99.79 \pm 0.38\%$  in the  $H-V$  basis and  $98.11 \pm 1.16\%$  in the  $A-D$  basis. The data in Fig. 2 were taken using a circular aperture with a full collection divergence angle of  $\sim 13$  mrad. From the singles count rate of  $\sim 1,600/s$  we infer a  $\sim 9.5\%$  conditional detection probability, limited in large part by the Si APD detector efficiency of  $\sim 50\%$ , the IF transmission of  $\sim 36\%$  (60% peak transmission and 60% double-Lorentzian filter shape), and the measured 95% transmission efficiency through the other optical components. The remaining reduction in the conditional detection probability can be attributed to spatial filtering that was provided by the 2-mm diameter aperture, which is a typical problem due to the multimode nature of SPDC with an unfocused or weakly focused pump [9]. We measured a Si APD dark-count rate of  $\sim 50/s$ , and the non-parametric fluorescence counts were less than 5% of the measured singles which, at this pump level, did not contribute to any accidental coincidences.

Figure 3 shows the quantum interference measurements at a pump power of 1.1 mW and with all other parameters being the same as in Fig. 2. The singles rate increased to  $16,000 s^{-1}$  at this power level, and the quantum-interference visibilities are found to be  $98.04 \pm 0.35\%$  in the  $H-V$  basis and  $96.64 \pm 0.46\%$  in the  $A-D$  basis. From the singles count rate and the 9.5% conditional detection probability, one can estimate the pair generation rate to be 1.1% per pulse. This high pump power caused the slight reduction in visibilities due to multiple-pair emission events, which are analyzed in detail in the next section.

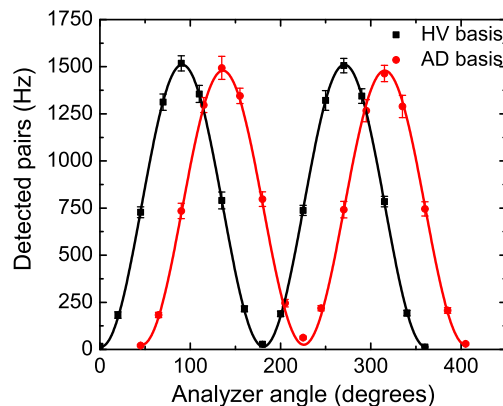


FIG. 3: (Color online) Quantum interference measurements for input pump of 1.1 mW and sinusoidal fits in the  $H-V$  (squares) and  $A-D$  (circles) bases. With slightly higher photon pair generation rates, we obtain 98.04%  $H-V$  visibility and 96.64%  $A-D$  visibility.

We have also measured the variation in the quantum-interference visibility at different divergence angles, as set by the aperture diameters, and at a constant input power of 1.1 mW. For each data point in Fig. 4, we average 30 1-s measurements of  $C_{\max}$  and  $C_{\min}$ , and obtain the visibility calculated from Eq. (2). At a given

pump power a larger aperture size allowed more light to be collected which increased the effective pair generation rate. As a result, multiple-pair events increased (see next section for details) and caused the visibility to degrade slightly, as shown in Figure 4 for the measurements in the  $H$ - $V$  (squares) basis. The  $A$ - $D$  data shows a more pronounced deterioration in the visibility at larger collection angles. The  $H$ - $V$  basis was the natural basis aligned with the PPKTP's crystal principal axes. Therefore, measurements in the  $A$ - $D$  basis required the coherent superposition of the two counter-propagating down-converter outputs, and the entanglement quality was sensitive to their spatial mode distinguishability and to the phase variation of the output state across the spatial extent. In our case, the  $A$ - $D$  data in Fig. 4 clearly show that the singlet-state entangled output of the PSI degraded at larger divergence angles. In designing the Sagnac source for a specific application, one must therefore consider the trade-off between generation efficiencies and entanglement quality as a function of the collection angles.

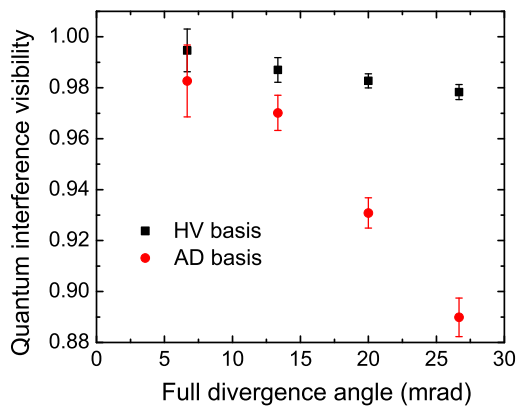


FIG. 4: (Color online) Quantum interference visibilities in the  $H$ - $V$  (squares) and  $A$ - $D$  (circles) bases for various aperture sizes at a constant input pump power of 1.1 mW.

### B. CHSH $S$ -parameter measurements

Violation of the CHSH form of Bell's inequality [20] is another common method of entanglement characterization by measuring its  $S$  parameter. For an ideal entangled state a maximum value of  $S = 2\sqrt{2}$  is predicted by quantum mechanics, whereas  $S$  cannot be greater than 2 classically. Therefore, the state is considered nonclassical if  $2 < S \leq 2\sqrt{2}$  and the closer  $S$  is to  $2\sqrt{2}$ , the higher is the entanglement quality. We follow the measurement procedure of Ref. [7]. The  $S$ -parameter is given by four measurement expectation values [20]

$$S = |E(\theta_S, \theta_I) + E(\theta_S, \theta'_I) - E(\theta'_S, \theta_I) + E(\theta'_S, \theta'_I)|, \quad (3)$$

where  $\theta_S$  and  $\theta_I$  are the polarization analyzer angles for signal and idler, respectively. We chose to maximize  $S$  by using  $\theta_S = -\pi/4$ ,  $\theta'_S = 0$ ,  $\theta_I = 5\pi/8$ , and  $\theta'_I = 7\pi/8$ . Each expectation value  $E(\theta_S, \theta_I)$  is obtained from coincidence measurements in 4 different polarization analyzer combinations: the chosen signal and idler set and their orthogonal sets:  $(\theta_S, \theta_I)$ ,  $(\theta_S, \theta_I + \pi/2)$ ,  $(\theta_S + \pi/2, \theta_I)$  and  $(\theta_S + \pi/2, \theta_I + \pi/2)$ . One calculates the expectation value according to

$$E(\theta_S, \theta_I) = \frac{C_{++} - C_{+-} - C_{-+} + C_{--}}{C_{++} + C_{+-} + C_{-+} + C_{--}}, \quad (4)$$

where the subscript  $(++)$  represents the angle set  $(\theta_S, \theta_I)$  and the  $(-)$  subscript substitutes it with the orthogonal angle.

We made the  $S$ -parameter measurements for the low-flux case with an input pump power of  $\sim 70 \mu\text{W}$  at a full divergence angle of 13 mrad. A total of 16 coincidence measurements was made, each consisting of an average of 30 1-s data sets. We obtain  $S = 2.739 \pm 0.119$ , indicating a violation of Bell's inequality of more than 6 standard deviations. The entanglement quality given by  $S$  is comparable to that indicated by the quantum-interference visibility measurements.

### C. Quantum state tomography

A more detailed characterization of the output state can be obtained by quantum state tomography. One can reconstruct the density matrix,  $\rho$ , for a two-photon output state through a series of projective measurements. The coincidence counts recorded in these measurements can be used to obtain individual density matrix elements by a maximum likelihood algorithm. We utilize the protocol outlined in [23, 24], to estimate  $\rho$  from 16 projective measurements for an input pump power of 0.1 mW at a full divergence angle of 13 mrad. For each projective measurement, we averaged 30 1-s coincidence counting data points. Coincidence data from these measurements are used in a nonlinear least squares algorithm to estimate the bipartite density matrix from which fidelity measures can be calculated. The real and imaginary parts of  $\rho$  are plotted in Fig. 5. This density matrix estimation yields 98.85% fidelity for the PSI singlet state output, where fidelity is calculated as  $\text{Tr}\{\rho\rho_{\psi^-}\}$ , with  $\rho_{\psi^-}$  being the singlet state density operator. Another entanglement measure, tangle, is calculated from the measurements to be 0.9589, where a factorizable state yields zero tangle and a maximally-entangled Bell state yields unity. We observe that all three types of measurements are equally effective and useful in characterizing the PSI output state as highly entangled.

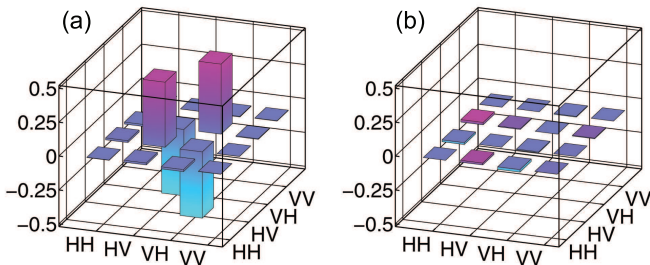


FIG. 5: (Color online) Quantum state tomography of PSI singlet-state output showing (a) real and (b) imaginary parts of the density matrix. An optimization routine uses a non-linear least squares algorithm to estimate individual matrix elements from 16 projective measurements under different polarization analyzer settings. Singlet-state fidelity is calculated as 98.85%. The density matrix yields a tangle of 0.9589.

#### IV. HIGH-FLUX CHARACTERISTICS

In the previous section the Sagnac SPDC source output has been characterized in the low-flux limit. From the Fig. 3 measurements we have determined that the pair generation rate was 1% per pulse per mW of average pump power for a full divergence angle of 13 mrad. Availability of over 400 mW pump power gives us the capability to drive the SPDC process at a significant generation rate at which multiple pairs could be produced in large numbers. This generation capability allows one to tailor the SPDC source for a specific application. One may, for instance, improve the entanglement source performance by increasing the pump power and reducing the divergence angle to achieve the desired generation rate with a higher entanglement quality. However, a higher flux output comes with its disadvantages. The main concern is an increase of accidental coincidences that reduces quantum-interference visibility, leading to potential errors in quantum information processing tasks. Take entanglement-based QKD as an example, while a higher secret key rate can be obtained for a mean pair generation number  $\alpha \gg 1\%$ , the maximum  $\alpha$  that can be used without compromising its security depends on a number of operational system parameters [19]. As a result, it is highly useful to have a simple and accurate estimate of the pair generation rate under all circumstances. In this section, we will consider the occurrence of accidental coincidences and how a pulsed source can lead to more errors than a cw source. We will also concentrate on the effect of multiple pair generation on entanglement quality and how that effect can be utilized to measure the pair generation probability accurately.

#### A. Accidental coincidences

There are three main contributions to the observation of accidental coincidences in the typical measurement setup of Fig. 1. The first type of contribution is due to the generation of independent multiple entangled pairs from a multimode SPDC source under strong pumping. If the detected coincident photon pair originates from two different signal-idler pairs, there is no polarization correlation and therefore an error may occur. Considering the case of two-pair events, the production rate is proportional to the square of the pump power. The second type of contribution is caused by the detection of one photon from a down-converted photon pair and a UV-induced fluorescence photon emitted by the PP-KTP crystal which we measured to have a generation rate of less than 5% of the singles count rate. Since the fluorescence varies linearly with the pump power, the accidental coincidence rate is proportional to the square of the pump power. There is also the possibility of an accidental coincidence due to the detection of two fluorescence photons, but the probability is much lower than the case when one of the detected photons belongs to a down-converted pair. The third contribution comes from background photons from stray light and from detector dark counts. Both events are independent of the pump power and generally the background and dark counts are low enough that accidental coincidences caused by them are negligible.

The above discussion on accidental coincidences applies to both cw and pulsed SPDC. However, more accidental coincidences are observed in the pulsed case than in the cw case for the same average pumping power. If we assume the same SPDC setup, then the same average input power yields the same number of down-converted pairs per second for the cw and pulsed cases. In cw operation, the SPDC pair or fluorescence photon generation probability within a coincidence window of duration  $T_c$  is proportional to  $T_c$ . The cw accidental coincidence rate resulting from two-pair events is then given by  $f_{cw} = gT_c$ , where  $g$  is a proportionality constant. On the other hand, for pulsed SPDC with a repetition rate of  $R_p$ , the pair or fluorescence emission is localized within each pump pulse duration, whose width is typically smaller than  $T_c$ , as in our setup. Therefore, the SPDC pair (or fluorescence photon) generation probability per pulse (alternatively, per coincidence window) is proportional to  $1/R_p$ . The accidental coincidence probability per pulse is then proportional to  $1/R_p^2$ , and the accidental coincidence rate is  $f_{pulsed} = g/R_p$ . Note that the cw and pulsed cases have the same proportionality as long as the same type of accidental coincidences is considered. For the same input power, the ratio of their accidental rates is

$$\frac{f_{cw}}{f_{pulsed}} = R_p T_c. \quad (5)$$

Using a typical value for the coincidence window du-

ration  $T_c = 1$  ns, the repetition rate of  $R_p = 31.1$  MHz for our pulsed pump implies that  $f_{\text{cw}} \ll f_{\text{pulsed}}$ . That is, our pulsed system is much more susceptible to visibility degradation due to accidental coincidences compared with a cw source with the same entangled pair generation rate. Equivalently, the cw source can tolerate a much higher average pump power than a pulsed source ( $\sim 18\times$  in our case) for the same amount of accidental coincidences. This problem can be minimized by increasing the repetition rate until it is comparable to  $1/T_c$ . Increasing the repetition rate, however, has its own problems. For instance, typical Si APDs are not able to handle detection rates much higher than a few MHz. Also, it is not desirable to have  $R_p T_c > 0.5$  because of the need for temporal separation of the pulses. For a pulsed source designed for a specific application such as QKD, one must be aware of the trade-offs between the need for a high pair generation rate and the desire for high entanglement quality, and strike an application-specific balance for the appropriate combination of pump powers, repetition rates, detector speeds, and error budget.

## B. Multiple-pair generation

The UV-induced fluorescence rate was measured by detuning the phase matching temperature so that only fluorescence photons were detectable and we found that it was only a small fraction ( $\sim 5\%$ ) of the detected singles rate. Therefore multiple-pair generation is the main contributor to accidental coincidences in our setup. The limitations due to multi-pair events have previously been observed [25, 26]. Eisenberg *et al.* measured the multi-pair visibility degradation in their study of stimulated parametric emission in a multi-pass down-conversion configuration [27]. In this section we use a simple model to quantify the effect of multiple-pair generation on two-photon quantum interference measurements in spontaneous parametric emission in a single-pass down-conversion setup. We compare the theoretical predictions to our experimental observations at high pump powers.

Consider an ideal pulsed SPDC source that generates singlet-state polarization-entangled photon pairs, and there are no background or fluorescence photons. We assume that the free-space output is spatially multimode and that the output is also temporally multimode because the coincidence measurement time is large compared with the output pulse width. The number of entangled pairs in the output pulse is Poisson distributed with a mean pair generation number  $\alpha$ :

$$p_n(\alpha) = \frac{e^{-\alpha} \alpha^n}{n!}, \quad \sum_{n=0}^{\infty} p_n(\alpha) = 1, \quad (6)$$

where  $p_n(\alpha)$  is the probability weight for obtaining exactly  $n$  pairs per pulse. We further assume that the  $n$  entangled pairs are independent because of the multimode nature of the output. That is, each mode has an

occupation number of either 0 or 1. We note that the assumption of the Poisson distribution is not valid for single-mode outputs, but we have found that the results below do not change significantly when we replace it with a thermal distribution.

We focus on the effect of multiple pairs on the two-photon quantum-interference visibility. In calculating the visibility of Eq. (2), we only need to obtain the maximum and minimum coincidence probabilities,  $C_{\text{max}}$  and  $C_{\text{min}}$ , respectively. For singlet-state entangled output, we consider a coincidence measurement along  $H$  polarization for the signal photon and along  $V$  ( $H$ ) polarization for the idler photon to measure  $C_{\text{max}}$  ( $C_{\text{min}}$ ), and we assume ideal polarization analyzers. Other polarization settings (such as  $A$ - $D$ ) work just as well, as long as the polarizers are orthogonal for measuring  $C_{\text{max}}$  and parallel for measuring  $C_{\text{min}}$ . To complete the model for the calculations, we further assume ideal photon-number non-resolving detectors and both the signal and idler paths have a system detection efficiency  $\eta$ .

The minimum and maximum coincidence probabilities are given by

$$C_{\text{min}} = \sum_{n=1}^{\infty} p_n(\alpha) c_{\text{min}}(n), \quad (7)$$

$$C_{\text{max}} = \sum_{n=1}^{\infty} p_n(\alpha) c_{\text{max}}(n), \quad (8)$$

where  $c_{\text{min}}(n)$  and  $c_{\text{max}}(n)$  are the minimum and maximum coincidence probabilities for an output with exactly  $n$  pairs of entangled photons. Note that the summation starts from  $n = 1$  because  $c_{\text{min}}(0) = c_{\text{max}}(0) = 0$ . For  $n$  independent photon pairs, there are  $(n + 1)$  different ways to arrange their polarization orientations relative to the analyzer settings, and they follow the binomial distribution. For example, the  $n$  signal photons may be  $H$ -polarized for  $k$  of them (with corresponding  $V$ -polarized idler photons), and  $V$ -polarized for the rest, or  $n - k$  of them, and it has a probability of  $\binom{n}{k}/2^n$  with the binomial coefficient

$$\binom{n}{k} = \frac{n!}{(n-k)!k!} \quad (9)$$

for  $0 \leq k \leq n$ . For a given polarization arrangement, one requires at least one detected  $H$ -polarized event at the signal detector and at least one detected  $V$ -polarized event at the idler detector to yield a coincidence count for  $c_{\text{max}}(n)$ . Similarly, to obtain  $c_{\text{min}}(n)$  it is required to detect an  $H$ -polarized event at each detector. Combining the above requirements we obtain

$$\begin{aligned} c_{\text{min}}(n) &= \frac{1}{2^n} \sum_{k=1}^{n-1} \binom{n}{k} [1 - (1 - \eta)^k] [1 - (1 - \eta)^{n-k}], \\ c_{\text{max}}(n) &= \frac{1}{2^n} \sum_{k=1}^n \binom{n}{k} [1 - (1 - \eta)^k]^2. \end{aligned} \quad (10)$$

The above coefficients allow us to compute the minimum and maximum coincidence probabilities from Eqs. (7-8) and obtain the visibility of Eq. (2) as a function of the mean pair generation probability per pulse  $\alpha$ .

It is instructive to evaluate the multiple-pair effect for small  $\alpha$  in which case we ignore terms with more than two pairs of entangled photons and simplify the Poisson distribution coefficients  $p_1(\alpha) \approx \alpha(1 - \alpha)$  and  $p_2(\alpha) \approx \alpha^2/2$ . In this case, we obtain

$$C_{\min} = \frac{1}{4}\eta^2\alpha^2, \quad (11)$$

$$C_{\max} = \frac{1}{2}\eta^2\alpha \left[ 1 + \frac{\alpha}{4}(2 - 4\eta + \eta^2) \right], \quad (12)$$

and one obtains the visibility to the first order of  $\alpha$  as

$$V = 1 - \alpha. \quad (13)$$

The linear dependence of the quantum-interference visibility on the mean pair generation probability shows clearly how the entanglement quality degrades with increasing pump powers. It is a little surprising to see in Eq. (13) that there is no dependence on the system detection efficiency  $\eta$ . A physical explanation is that for a pair of photons that survive the system loss and are detected, one does not know if they belong to the same entangled pair or not and therefore it should only depend on the generation statistics and not on the system loss. For a system with high loss that results in a low detection rate the entanglement quality may still be compromised by multi-pair events.

The above results can be directly compared with measurements using our setup in Fig. 1. The free-space output of our pulsed Sagnac source with a weakly focused pump had many spatial modes that can be described by a Poisson distribution. Moreover, the pumping rate was low enough that even at the highest measured  $\alpha$  value in the experiment, stimulated emission can be neglected. We measured quantum-interference visibilities in both  $H$ - $V$  and  $A$ - $D$  bases at different input pump powers and at a fixed full divergence angle of 13 mrad. The pair generation rate per pulse  $\alpha$  is inferred from singles and coincidence measurements, which have yielded a conditional detection efficiency of  $\eta = 9.5\%$  under these operating conditions. The maximum pump power was  $\sim 70$  mW which corresponds to  $\alpha = 0.7$ . We measured  $\sim 110,000$  pairs/s with  $\sim 1$  MHz singles rate at this power level. We did not use higher  $\alpha$  values to avoid any possible crystal damage at elevated pump power levels.

Figure 6 plots the measured visibilities and compares them with our calculated values. The  $H$ - $V$  results match the theoretical values very well in both the low and high  $\alpha$  regimes. In particular, at low  $\alpha$ , the visibility degradation is linear with respect to the mean pair generation number. The  $A$ - $D$  results also show the expected linear dependence on  $\alpha$  except there is a fixed amount of visibility loss, which is related to other factors. We speculate that the discrepancy between the  $H$ - $V$  and  $A$ - $D$

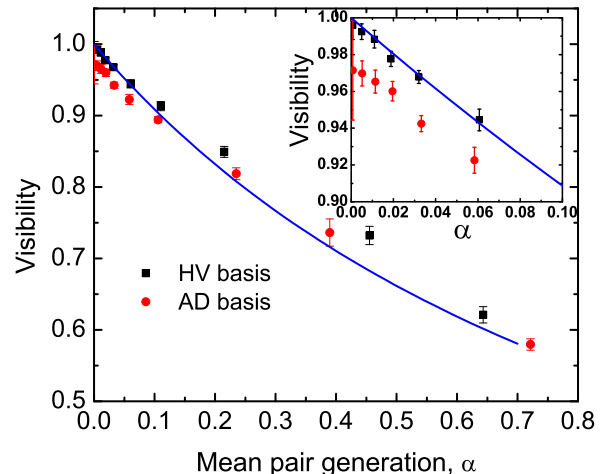


FIG. 6: (Color online) Quantum-interference visibility in the  $H$ - $V$  (squares) and  $A$ - $D$  (circles) bases as a function of mean pair generation number  $\alpha$ . The solid curve is computed from our theoretical model. Visibilities in the  $A$ - $D$  basis are lower than those in the  $H$ - $V$  basis due to other factors that are unrelated to multi-pair occurrences. Inset shows the linear behavior of the quantum interference visibility in the low-flux regime ( $\alpha \leq 0.1$ ).

visibilities is due to wavefront distortion in the optical components of the Sagnac interferometer that created partial spatial distinguishability. We have verified that this problem did not originate from the input pump profile because we observed no visibility improvement after we cleaned up the pump spatial mode by coupling it into a single mode fiber. At this point, we suspect that the surface quality of the PBS was responsible for the visibility loss. Further testing with a higher quality dual-wavelength PBS is needed to support this claim. Since the  $H$ - $V$  measurements were made in the down-converters' natural polarization basis, their results were not affected by these distinguishability issues. It is useful to note that one can take advantage of the  $\alpha$  dependence of  $H$ - $V$  visibility measurements to deduce accurately the mean pair generation probability  $\alpha$ .

## V. DISCUSSION

We have presented a compact, pulsed, narrowband source of polarization-entangled photons that is of interest to entanglement-based free-space QKD. Pumped by a home-built, narrowband, pulsed UV source the Sagnac geometry ensures phase-stable generation of any desired Bell state at the degenerate wavelength of 780.7 nm. In principle, the bidirectionally pumped single-crystal Sagnac configuration eliminates spatial, spectral, and temporal distinguishability in the interferometric combination of the two counter-propagating down-converter outputs. Experimentally, we observed high quality en-



tanglement except for a slight quantum interference visibility loss caused probably by the spatial distinguishability problem. Pulsed operation allows a QKD system to easily manage the arrival times of the photons by synchronization of the transmitter and receiver clocks. It also provides temporal discrimination against background light that arrives outside of the clocked coincidence window. The narrowband SPDC output allows a matching narrowband spectral filter to be used to screen out ambient light especially during daylight QKD operation.

Our pulsed Sagnac source is highly efficient and it can be pumped to have a significant pair generation per pulse, producing 0.01 pair per pulse at an average pump power of  $\sim 1$  mW at a pump repetition rate of 31.1 MHz. We show that at high pair generation the presence of multiple pairs degrades the two-photon entanglement quality that may not be desirable in some quantum information processing tasks. If the pair generation probability per pulse is limited by multi-pair events, then the only way to increase the flux without reducing the entanglement quality is to increase the repetition rate, up to the point where the detector speed may impose a practical limit.

It is common to evaluate the performance of a cw SPDC source by its quantum-interference visibility and its spectral brightness, which is the number of detected pairs per second per mW of pump in a 1-nm bandwidth. However, the spectral brightness is not an appropriate performance metric for a pulsed source. Instead of spectral brightness, it is more useful to specify the pair generation probability per pulse and the repetition rate of the source. With the high power pumping capability, we

have observed the quantum interference visibility as a function of pair generation rate and reached an  $\alpha$  value as high as 0.7. The pulsed Sagnac source is capable of achieving a high enough pair generation rate for optimal secret key generation in an entanglement-based QKD system in the presence of channel losses and non-ideal detection efficiencies [19]. High pair generation rates have been reported for fiber-based  $\chi^{(3)}$  downconversion sources [26, 28]. Our system performance compares well in terms of achievable generation efficiency with negligible amount of fluorescence and scattering effects.

In conclusion, we have developed a highly efficient SPDC source utilizing the Sagnac configuration to generate pulsed, narrowband, polarization-entangled photons. We have demonstrated high entanglement quality and high pair generation rates with the Sagnac source. Under strong pumping, the pulsed source shows entanglement quality degradation due to multi-pair events, in accordance with our theoretical analysis. The source can be utilized in many quantum information processing applications including quantum key distribution. In addition, because of its high efficiency and compactness, the Sagnac source is also useful for more advanced quantum enabling technologies such as an on-demand source of single photons [29].

#### Acknowledgments

This work was supported by the Disruptive Technologies Office through a National Institute of Standards and Technology contract 60NANB5D1004.

- 
- [1] E. Knill, R. Laflamme, and G. J. Milburn, *Nature* **409**, 46 (2001).
  - [2] D. Bouwmeester, J. W. Pan, K. Mattle, M. Eibl, H. Weinfurter, and A. Zeilinger, *Nature* **390**, 575 (1997).
  - [3] A. K. Ekert, *Phys. Rev. Lett.* **67**, 661 (1991).
  - [4] P. G. Kwiat, K. Mattle, H. Weinfurter, A. Zeilinger, A. V. Sergienko, and Y. Shih, *Phys. Rev. Lett.* **75**, 4337 (1995).
  - [5] M. Fiorentino, G. Messin, C. E. Kulewicz, F. N. C. Wong, and J. H. Shapiro, *Phys. Rev. A* **69**, 041801(R) (2004).
  - [6] J. B. Altepeter, E. R. Jeffrey, and P. G. Kwiat, *Opt. Express* **13**, 8951 (2005).
  - [7] T. Kim, M. Fiorentino, and F. N. C. Wong, *Phys. Rev. A* **73**, 012316 (2006).
  - [8] F. N. C. Wong, T. Kim, and J. H. Shapiro, *Laser Phys.* **16**, 1517 (2006).
  - [9] A. Fedrizzi, T. Herbst, A. Poppe, T. Jennewein, and A. Zeilinger, *Opt. Express* **15**, 15377 (2007).
  - [10] Y.-H. Kim, S. P. Kulik, and Y. Shih, *Phys. Rev. A* **62**, 011802(R) (2000).
  - [11] J. F. Hodelin, G. Khoury, and D. Bouwmeester, *Phys. Rev. A* **74**, 013802 (2006).
  - [12] M. Fiorentino, C. Santori, S. M. Spillane, R. G. Beausoleil, and W. J. Munro, *Phys. Rev. A* **75**, 032334 (2007).
  - [13] P. G. Kwiat, P. H. Eberhard, A. M. Steinberg, and R. Y. Chiao, *Phys. Rev. A* **49**, 3209 (1994).
  - [14] J. H. Shapiro and N. C. Wong, *J. Opt. B* **2**, L1 (2000).
  - [15] B.-S. Shi and A. Tomita, *Phys. Rev. A* **69**, 013803 (2004).
  - [16] O. Kuzucu, F. N. C. Wong, D. E. Zelmon, S. M. Hegde, T. D. Roberts, and P. Battle, *Opt. Lett.* **32**, 1290 (2007).
  - [17] N. Kiesel, C. Schmid, G. Tóth, E. Solano, and H. Weinfurter, *Phys. Rev. Lett.* **98**, 063604 (2007).
  - [18] M. Eibl, N. Kiesel, M. Bourennane, C. Kurtsiefer, and H. Weinfurter, *Phys. Rev. Lett.* **92**, 077901 (2004).
  - [19] X. Ma, C.-H. F. Fung, and H.-K. Lo, *Phys. Rev. A* **76**, 012307 (2007).
  - [20] J. F. Clauser, M. A. Horne, A. Shimony, and R. A. Holt, *Phys. Rev. Lett.* **23**, 880 (1969).
  - [21] J. E. Nordholt, R. J. Hughes, G. L. Morgan, C. G. Peterson, and C. C. Wipf, *Free-Space Laser Communication Technologies XIV* **4635**, 116 (2002).
  - [22] T. Kim, M. Fiorentino, P. V. Gorelik, and F. N. C. Wong (2005), arXiv:physics/0501141v1.
  - [23] D. F. V. James, P. G. Kwiat, W. J. Munro, and A. G. White, *Phys. Rev. A* **64**, 052312 (2001).
  - [24] J. B. Altepeter, E. R. Jeffrey, and P. G. Kwiat, in *Advances in Atomic, Molecular and Optical Physics*, edited by P. Berman and C. Lin (Elsevier, 2005), vol. 52,

chap. 2.

- [25] H. de Riedmatten, I. Marcikic, W. Tittel, H. Zbinden, and N. Gisin, *Phys. Rev. A* **67**, 022301 (2003).
- [26] C. Liang, K. F. Lee, T. Levin, J. Chen, and P. Kumar, *Opt. Express* **14**, 6936 (2006).
- [27] H. S. Eisenberg, G. Khoury, G. A. Durkin, C. Simon, and D. Bouwmeester, *Phys. Rev. Lett.* **93**, 193901 (2004).
- [28] J. Fan, M. D. Eisaman, and A. Migdall, *Phys. Rev. A* **76**, 043836 (2007).
- [29] J. H. Shapiro and F. N. C. Wong, *Opt. Lett.* **32**, 2698 (2007).